Dental Materials Journal 2023; 42(2): 273–281

Evaluation of the machinability and machining accuracy of polymer-based CAD/CAM blocks using merlon fracture test model

Chang-Sub JEONG[1,2], Joon-Mo MOON[1], Hee-Jeong LEE[1], Ji-Myung BAE[1], Eun-Joo CHOI[3], Sung-Tae KIM[4], Youngbum PARK[5] and Seunghan OH[1]

[1] *Department of Dental Biomaterials and the Institute for Biomaterials and Implant, College of Dentistry, Wonkwang University, Iksan 54538, Republic of Korea*
[2] *Department of Dental Laboratory Technology, Faculty of Health and Medical Sciences, Wonkwang Health Science University, Iksan 54538, Republic of Korea*
[3] *Department of Oral and Maxillofacial Surgery, College of Dentistry, Wonkwang University, Iksan 54538, Republic of Korea*
[4] *Department of Periodontology, Dental Research Institute, School of Dentistry, Seoul National University, Seoul 03080, Republic of Korea*
[5] *BK21 Plus Project, Oral Science Research Center, Department of Prosthodontics, Yonsei University College of Dentistry, Seoul 03722, Republic of Korea*
Corresponding author, Seunghan OH; E-mail: shoh@wku.ac.kr

The aims of this study were to estimate the machinability and machining accuracy of polymer-based CAM blocks using the merlon fracture test model specified in ISO 18675: 2022. Three hybrid disc blanks (MazicDuro, HC Disk, and Enamic) and three polymethyl methacrylate (PMMA) disc blanks (PMMA Disk, PMMA Block, and MazicTemp Hybrid) were tested in this study. The machinability was evaluated by assigning scores according to the fracture range of merlons with areas divided by ten vertical planes. The machining accuracy was evaluated by superimposing methods *via* CAD reference data and CAD specimen data. Within the limits of this study, a thickness of 0.3 mm is recommended for the clinical application of polymer-based CAD/CAM blocks in dental restorations that require superior machinability and accuracy. In addition, the machinability and machining accuracy tests of polymer-based CAM blocks are expected to provide guidelines for preparing accurate dental restorations.

Keywords: Polymer-based CAM block, Machinability, Machining accuracy, CAD/CAM

INTRODUCTION

Polymer-based computer-aided manufacturing (CAM) blocks have been widely used in dental computer-aided design (CAD)/CAM systems because they provide affordable machinability compared to ceramic blocks and are effective for indirect dental restorations[1-4]. Polymer-based CAM blocks are generally classified as polymethyl methacrylate (PMMA)-based and hybrid composite resin-based polymers[5]. As the PMMA blocks are prepared using high-temperature and high-pressure processes, their mechanical properties and biocompatibilities are better than those of conventional PMMA materials, which display polymerization shrinkage, discoloration, and high residual monomer contents[6-9]. These blocks are widely used for provisional restoration, denture bases, artificial teeth for full dentures[10], frames for partial dentures[11], and splints for temporomandibular joint rehabilitation[12]. For CAM applications, the hybrid composite resin blocks maximize the advantages of ceramic and resin materials and show improved physical and chemical properties compared to conventional composite resins[13-16]. According to the chemical structures of ceramic and resin materials, the hybrid blocks are classified as resin nanoceramic (RNC) structures and polymer infiltrated ceramic network (PICN) structures. An RNC structure is composed of a well-dispersed ceramic nanofiller and a highly polymerized resin matrix, while a PICN structure consists of a polymerized UDMA and TEGDMA mixture infiltrated into a pre-sintered inorganic ceramic support. Thus, the main chemical structure of RNC is polymer, but that of PICN is ceramics. Compared with ceramic blocks, hybrid composite resin blocks have the advantages of short processing periods, long milling bur lifetimes, and excellent machinability[17].

The subtractive manufacturing (SM) technology, wherein block-shaped materials are machined with a milling tool using a numerically controlled milling machine[18], is the most common dental CAD/CAM method. Several factors affect the accuracy of the final dental products prepared by SM processes. Among them, the machinability of CAM blocks plays an essential role in the accuracy of machined dental prostheses and is not considered in conventional processes for dental prosthesis fabrication. The accuracy of a dental restoration is an important clinical factor for the success of a dental treatment, and it is evaluated using the fit of a marginal and internal region of a dental prosthesis[19]. A poor marginal fit caused by the low accuracy of a prosthesis could lead not only to the fracture of a dental product by inducing local stress during tooth mastication[20,21] but also to an adverse effect on periodontal tissue, resulting in periodontal disease[22,23]. Therefore, the surface defects and roughness of a machined dental prosthesis generated during the SM process are crucial parameters for the accuracy of the dental prosthesis[17,24,25].

Most machinability-based studies have conducted chipping factor assessments[26-28], and the accuracy

Received Jul 7, 2022: Accepted Nov 1, 2022
doi:10.4012/dmj.2022-154 JOI JST.JSTAGE/dmj/2022-154

of machined dental prostheses has mainly been investigated by performing marginal and internal fit tests of machined crowns[29-32]. However, few studies have simultaneously estimated the machinability and accuracy of CAM blocks. Recently, the merlon fracture test has been introduced in "ISO 18675: 2022-Dental–Machinable Ceramic Blank"[33] and is equally applicable to the international standard under development, including the evaluation of the machinability of polymer-based blanks[34]. This test can perform a quantitative evaluation of the machinability of ceramic-based dental prostheses manufactured in CAD/CAM systems. The shape of the merlon fracture test model is similar to a single crown with one bottom and four divided walls (merlon). ISO 18675 shows that the thickness of the model varies from 0.1 mm to 0.5 mm, and the merlon fracture test was evaluated by measuring the degree of fracture per merlon and determining the passing or failure of each specimen. We found that the merlon fracture test in ISO 18675 is somewhat insufficient for a detailed machinability evaluation as it is a relatively simple method of evaluating partial fractures with a trisected plane per merlon. Therefore, we decided to perform a more detailed machinability evaluation by subdividing the partial fracture evaluation into ten equal planes per merlon.

Previous CAD/CAM-based accuracy evaluation studies have mostly determined the fitting accuracy with an abutment and a prepared dental prosthesis using the indirect silicone replica method[14,35-37]. Thus, the obtained fitting accuracies are affected by the friction between the dental prosthesis and abutment, application load, and position of the dental prosthesis[38,39]. On the contrary, a superimposing method between the CAD reference and specimen data has been widely used to perform three-dimensional (3D) shape analysis of the fabricated samples *via* CAD/CAM systems[40-42]. Particularly, this method facilitates a structural analysis of the location of the polymer blanks subjected to machining damage to ascertain the degree of the local position of deformation that is generated while the composite resin blank is being machined. The brief experimental procedure of the superimposing method is as follows: After preparing the specimen with CAD reference data (CRD), it is scanned to acquire CAD specimen data (CSD). Then, the accuracy of the fabricated samples is measured by superimposing the CRD on the CSD and calculating the difference between the two data sets using 3D image analysis software. Studies based on the superimposing method use a denture model with general teeth and oral shapes. In the case of a denture model with a structure similar to that of a natural tooth, the method is applied in an actual clinical situation by evaluating the cutting accuracy of the dental prosthesis manufactured using the CAD/CAM system. However, owing to the complex and diverse shapes of denture models, it is difficult to derive standardized results using the superimposing method and locate specific parts of the samples that show machining errors. Thus, the standardized model is suitable for visually checking the errors in the machining process, as well as for evaluating the machining accuracy *via* the superimposing method.

In this study, we performed a machinability test using the merlon fracture test model and modified the measurement method to improve machinability evaluation. In addition, we examined the feasibility of this method for machining accuracy evaluation by calculating the machining accuracy of prepared samples through superimposing scanned test model data and reference data in a 3D image analysis program. The null hypotheses of this study are that there exist no significant differences in the (1) machinabilities and (2) machining accuracies of different dental polymer-based CAD/CAM blocks.

MATERIALS AND METHODS

Polymer-based CAM blocks and CAD/CAM systems

We used three hybrid composite resin-based disc blanks (MazicDuro (VMD), HC Disk (SHC), and Enamic (VEN)) and three PMMA-based disc blanks (PMMA Disk (YHP), PMMA Block (HPB), and MazicTemp Hybrid (VMT)). Detailed information about these blocks is presented in Table 1. We used the Zenotec CAM software (Ivoclar Vivadent/Wieland, Liechtenstein, Germany) and a Select S2 milling machine (Ivoclar Vivadent/Wieland) to mill all the CAM blocks. In addition, we used a round tungsten carbide milling bur with a diamond coating (diameters of 1.0 mm and 2.0 mm; Zenotec spezial Schleifer, Ivoclar Vivadent/Wieland) for the hybrid blocks and cutting-edged tungsten carbide milling bur (diameters of 1.0 mm and 2.5 mm; Zenotec spezial Fräser, Ivoclar Vivadent/Wieland) for the PMMA blocks. The large and small milling burs were used for rough and fine milling, respectively. Each milling bur was replaced after it was used to mill an entire CAM block.

Design of CAD reference data

We designed CRD in the STL file format using 3D software (AutoCAD, Autodesk, San Rafael, CA, USA) to prepare the merlon fracture test model specified in ISO 18675. As shown in Fig. 1(A), the designed model is round (9.5 mm in height and 10.0 mm in diameter) and consists of a closed structure on one side. The four vertical walls corresponding to the merlon are connected to the flat floor bottom, and the thicknesses of the merlon and bottom are 0.1, 0.2, and 0.3 mm. In addition, a column (1.0 mm in height and 2.0 mm in diameter) is placed on the lower body of the model to set up the reference point for 3D analysis and number the positions of the four merlons (See Fig. 1(B)).

Machinability test

To fabricate the merlon specimen, we input the CAD reference image file into the CAM software of the milling machine. We set the thicknesses of the merlon and bottom areas to 0.1, 0.2, and 0.3 mm. We set the occlusal area as the flat bottom area of the merlon model so that the insertion direction of the milling bur was parallel to the merlon wall. The distances between

Table 1 The information of the materials used in this study

Type	Product (Structure)	Group name	Resin component	Ceramic component	Ceramic fraction (wt%)	Lot number	Manufacturer
HYBRID	Mazic Duro (RNC[1])	VMD	Bis-GMA[3], TEGDMA[4]	Zirconia filler, Silica filler, Barium aluminosilicate,	80	DH0D64A2	VERICOM, ChunCheon, Korea
	HC Disk (RNC)	SHC	UDMA[5], TEGDMA	Silica powder, Micro-fumed silica, Zirconium silicate	61	072001	SHOFU, Kyoto, Japan
	Enamic (PICN[2])	VEN	UDMA, TEGDMA	feldspathic crystalline particles in glassy matrix.	86	56880	VITA, Bad Sackingen, Germany
PMMA	PMMA Disk	YHP	PMMA[6]	N/A	N/A	PB04	YAMAHACHI Dental, Aichi, Japan
	PMMA Block	HPB	PMMA	N/A	N/A	170320z 170403z 201029010	HUGE Dental, Rizhao,China
	Mazic Temp Hybrid	VMT	PMMA	Silica filler	N/A*	HT1331A2	VERICOM

*The detailed composition is unknown.
[1] Resin nano ceramic
[2] Polymer infiltrated ceramic network
[3] Bisphenol a glycidyl methacylate
[4] Triethylene glycol dimethacrylate
[5] Urethane dimethacrylate
[6] Polymethyl methacrylate

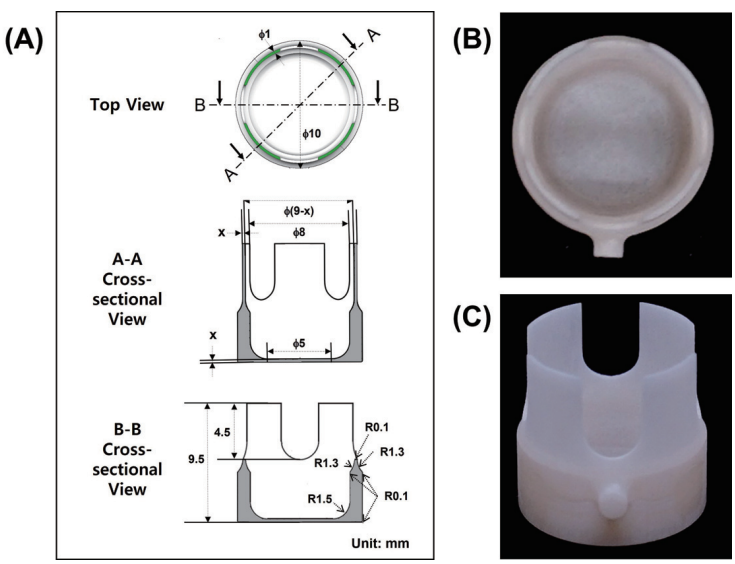

Fig. 1 Merlon fracture test model specified in ISO 18675; (A)Basic drawing, (B) top view, and (C) oblique view (x in (A): specific wall (merlon) thickness).

the manufactured samples in the disc blank were set to at least 2.0 mm to protect the specimen from impact during the milling process. In addition, we calibrated the machine before the milling process and followed

the instructions of the manufacturer for the machining strategy and parameters.

We prepared 90 specimens for six experimental groups (five samples per group) with three different thicknesses based on the merlon fracture test model. We evaluated the machinability of the specimens through microscopic examinations (S300II Olympus G20XT, Kikuchi, Nagano, Japan). We scored the intact subdivided walls in the merlon regions; this process is presented in detail in the evaluation of the machinability test shown in Fig. 2. The maximum score for each specimen was 40.

Machining accuracy test

The manufacturing process of the merlon specimens in the machining accuracy test was the same as that in the machinability test. We selected the intact machined specimens without wall damage from all the samples tested in the machinability test; four intact specimens with a thickness of 0.3 mm were selected. As most of the specimens with thicknesses of 0.1 mm and 0.2 mm were broken or damaged, they were not used for the machining accuracy test. First, we scanned the samples using a 3D scanning device (E4, 3Shape, Copenhagen, Denmark) to acquire the CSD. Then, we superimposed the CSD onto the CRD to calculate the root mean square (RMS) values using a 3D analysis program (Geomagic Control X, 3D Systems, Rock Hill, SC, USA). The formula for the RMS values calculated *via* 3D analysis is given below. All data points of the specimens were used for the calculation.

$$RMS=\frac{1}{\sqrt{n}}\cdot\sqrt{\sum_{i=1}^{n}(X_{1,i}-X_{2,i})^2}$$

Here, $X_{1,i}$ is the measurement point for CRD i, $X_{2,i}$ is the measurement point for CSD i, and n is the number of points used in the analysis. We visualized the deviation between CRD and CSD of the samples using color difference maps to visually examine the machining accuracy of the prepared samples.

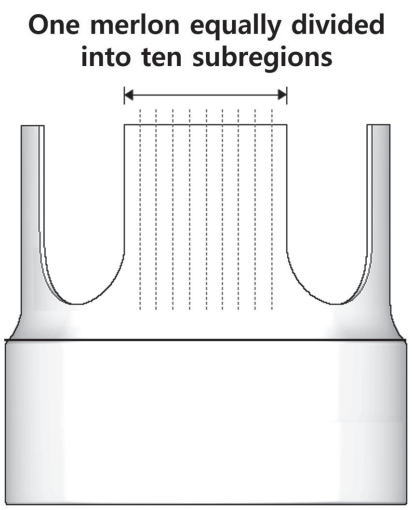

Fig. 2 Scoring method of the specimen for machinability evaluation.
The number of merlons per specimen=4, and maximum scores per specimen=40

Surface observation

Surface characterization was performed on the vertical walls of the merlon regions of the specimens, and these surfaces were machined in a direction parallel to the milling bur. The surfaces of the samples were observed using field emission scanning electron microscopy (FE-SEM; S4800, Hitachi High-Tech, Tokyo, Japan).

Statistical analysis

All machinability and machining accuracy test results were expressed in terms of the mean and standard deviation. One-way analysis of variance (ANOVA) was performed to evaluate statistically significant differences between the results. Additionally, the Games–Howell test was performed for *post-hoc* analysis. The significance level was α=0.05, and statistical processing was performed using the IBM SPSS 20 software (SPSS, Chicago, IL, USA).

RESULTS

Machinability test

Table 2 and Fig. 3 show the machinability scores for

Table 2 The machinability scores (mean ± standard deviation) of the experimental groups

No Unit

Group	Thickness	0.1 mm	0.2 mm	0.3 mm
Hybrid	VMD	10.2±1.92	36.8±0.83	39.0±0.70
	SHC	9.4±1.51	38.2±0.83	39.2±0.83
	VEN	25.8±2.86	38.8±0.83	39.2±0.83
PMMA	YHP	19.0±7.03	28.4±3.36	37.4±1.14
	HPB	24.0±3.60	32.2±0.83	37.2±0.83
	VMT	33.6±1.14	36.0±1.00	38.2±0.83

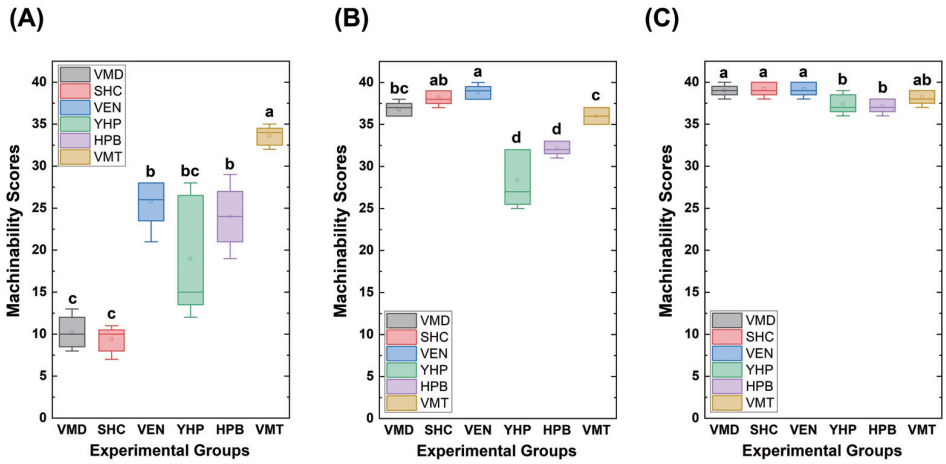

Fig. 3 Boxplots of the machinability scores of the experimental groups according to merlon thicknesses: (A) 0.1 mm, (B) 0.2 mm, and (C) 0.3 mm.
Different letters indicate statistical significances in each graph by one-way ANOVA at α=0.05.

Table 3 The RMS values (mean±standard deviation) of the experimental groups on the condition of 0.3 mm merlon thickness

Unit: μm

Group	Area	Total	Merlon	Bottom
Hybrid	VMD	24.80±1.13	25.40±1.40	23.86±1.34
	SHC	23.72±1.56	22.90±2.98	24.26±0.94
	VEN	31.08±2.06	31.04±2.90	31.32±1.46
PMMA	YHP	27.94±4.18	31.44±5.31	23.98±3.13
	HPB	31.70±5.31	35.00±6.01	28.16±4.72
	VMT	30.50±4.40	35.24±4.90	24.60±3.95

the three hybrid groups (VMD, SHC, and VEN) and three PMMA groups (YHP, HPB, and VMT) with different thicknesses. Most experimental specimens with a thickness of 0.3 mm are not chipped, and the machinability scores of all hybrid groups are statistically higher than those of the YHP and HPB groups (p<0.05). The score of the VEN group (38.8±0.83) is the highest at a thickness of 0.2 mm. In addition, the scores of the YHP (28.4±3.36) and HPB (32.2±0.83) groups are significantly lower than those of the other groups (p<0.05). The score of the VMT group (33.6±1.14) is the highest (p<0.05) at a thickness of 0.1 mm.

2. Machining accuracy test

Table 3 and Fig. 4 show the RMS values of the merlon, bottom, and total areas for all the experimental groups. The RMS value of the total specimen area for the SHC group (23.72±1.56 μm) is significantly lower than those for the VEN (31.08±2.06 μm) and HPB (31.70±5.31 μm) groups (p<0.05). The RMS values of the merlon area for the VMD (25.40±1.40 μm) and SHC (22.90±2.98 μm) groups are significantly lower than those for the HPB (35.00±6.01 μm) and VMT (35.24±4.90 μm) groups (p<0.05). The RMS values of the bottom area for the VMD (23.86±1.34 μm), SHC (24.26±0.94 μm), YHP (23.98±3.13 μm), and VMT (24.60±3.95 μm) groups are significantly lower than that for the VEN group (31.32±1.46 μm) (p< 0.05).

Figure 5 displays the deviation between CRD and CSD of the samples from each experimental group. The green, yellow, and dark yellow colors identified in the images represent the deviation range (green: deviation value≤30 μm; yellow: 30<deviation value≤60 μm; and dark yellow: 60<deviation value≤90 μm). The images of YHP, HPB, and VMT groups showed that a large portion of the merlon area and the bottom edge of the specimen were yellow. Also, the image of the VEN group indicated that yellow and dark yellow regions are observed at the lower part of the merlon area and the bottom edge of the specimen compared to the images of the VMD and SHC groups.

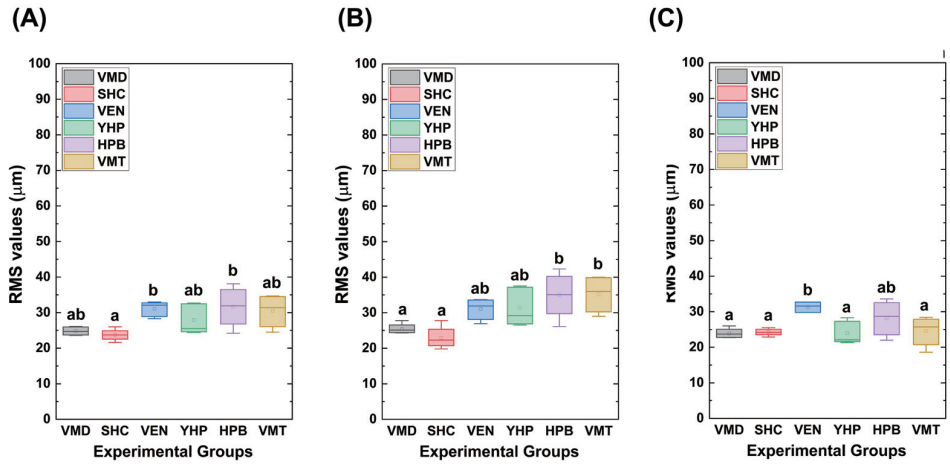

Fig. 4 Boxplots of the RMS values of the experimental groups at 0.3 mm merlon thickness; (A) total area, (B) merlon area, and (C) bottom area.
Different letters indicate statistical significances in each graph by one-way ANOVA at α=0.05.

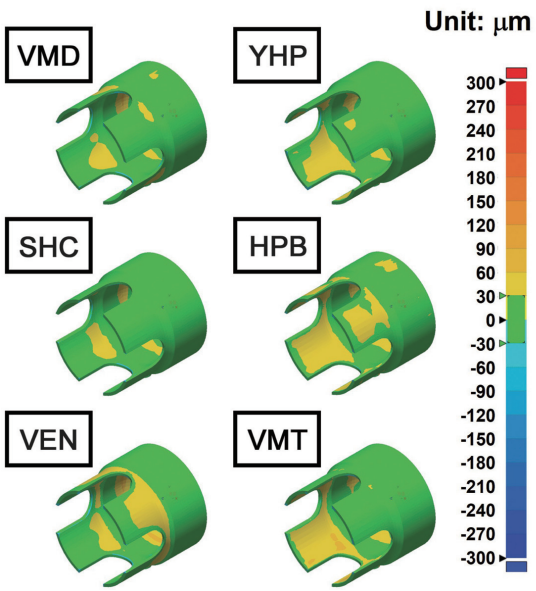

Fig. 5 Representative visualization images of the deviation between CAD reference data (CRD) and CAD specimen data (CSD) of the samples.

Surface observation

Figure 6 shows the FE-SEM images of the surfaces of the prepared specimens. From the low-magnification FE-SEM images, the stride lines from the machining trace can be observed on the surface for all the hybrid groups but not for the PMMA groups. High-magnification FE-SEM images show fractured particles on the surface of the VEN group. In addition, the PMMA groups display extremely even and smooth surfaces.

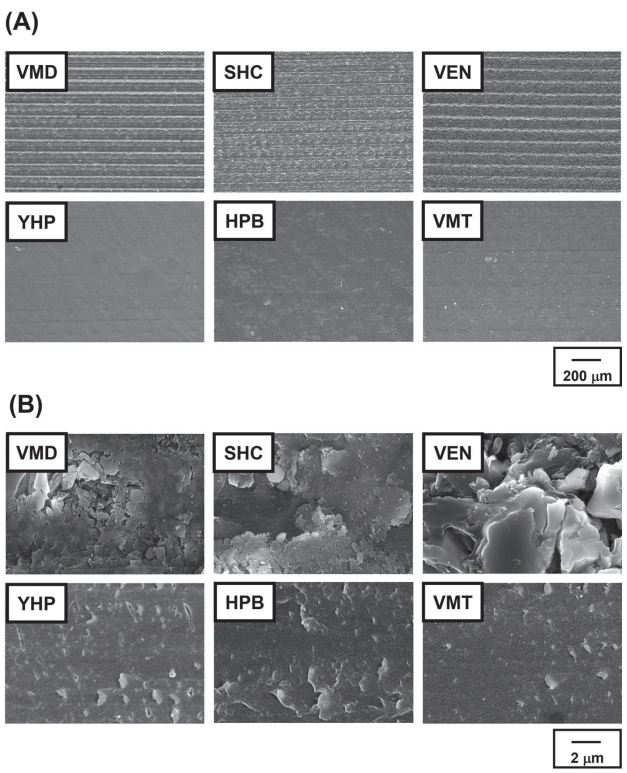

Fig. 6 FE-SEM images of the surface machined parallel to the milling bur of the experimental groups.
(A) Low magnification and (B) high magnification

DISCUSSION

Based on the results of the machinability and machining accuracy tests of polymer-based CAM blocks using the merlon fracture test model specified in ISO 18675, the

two null hypotheses established before the experiments were rejected. It was found that the thickness of dental prostheses manufactured in dental clinics is generally 0.5 mm or higher[43,44]; however, the marginal area of the dental prostheses —prone to chipping and microfractures— should be 0.5 mm thick or lower. Therefore, the thicknesses considered in this study (0.1, 0.2, and 0.3 mm) are appropriate for evaluating the machinability to simulate the condition of dental prosthesis fabrication.

All the experimental groups with a thickness of 0.3 mm exhibited excellent machinability. However, the hybrid and PMMA groups underwent chipping and fractured at thicknesses of 0.1 mm and 0.2 mm. We speculate that the inorganic fillers included in the CAM blocks play a critical role in their machinability. All the hybrid CAM blocks tested in this study contained more than 60 wt% inorganic materials (See Table 1) and exhibited exceptional mechanical properties, while the PMMA-based blocks contained either no inorganic fillers or small amounts of inorganic fillers. Thus, the difference between the machinabilities of the hybrid and PMMA groups appears to be caused by the difference between the mechanical properties at thicknesses of 0.2 mm and 0.3 mm. However, the opposite trend was observed in the machinability results for the hybrid and PMMA groups at a thickness of 0.1 mm. The FE-SEM images of all the experimental groups (See Fig. 5) demonstrated stride lines at regular intervals on the surfaces of the hybrid group specimens. These lines are expected to transmit the impact from the milling bur to the surface of the sample during machining. The hybrid CAM blocks, including inorganic fillers, exhibited superior mechanical properties and brittleness compared to the PMMA CAM blocks. Thus, the hybrid blocks showed excellent machinability without breakage up to a certain thickness. However, it is assumed that significant fractures can occur below a critical thickness (0.1 mm in this study) owing to high brittleness. At a thickness of 0.1 mm, the machinability of the VEN group was significantly higher than that of the VMD and SHC groups ($p<0.05$), which was presumed to be due to the structural differences in the hybrid CAM blocks. The VMD and SHC groups had an RNC structure, whereas the VEN group had a PICN structure.

Comparing the mechanical properties of the blank with the RNC structure to the blank with the PICN structure, Choi *et al.* reported that the flexural strength of the blank with the RNC structure is similar to that of the blank with the PICN structure. However, the elastic modulus of the blank with the RNC structure is lower than that of the blank with the PICN structure[45]. Although the blanks with RNC and PICN structures are hybrid materials, both have different chemical forms. As mentioned in the Introduction, the main frame of RNC structure is polymer, whereas PICN is ceramics. Therefore, it is reasonable that the blank with PICN structure exhibit ceramic characteristics in terms of mechanical properties. This difference in the moduli of elasticity is similar to that of the result of machinability in this study. Thus, we can confirm that the machinability of the blank is directly affected by the elastic modulus of the blanks.

From the results of the machining accuracy test, there were no significant errors (>100 μm in error) in the merlon and bottom regions. The VMD and SHC groups showed excellent machining accuracy in comparison with the other groups. These groups had RNC structures with good machinability at thicknesses of 0.2 mm and 0.3 mm. On the contrary, the VEN group, which had a PICN hybrid structure, showed low machining accuracy in the bottom area, which was milled in the direction perpendicular to the milling bur such that the end tip of the bur was in contact with the specimen. Thus, the VEN group, with high brittleness, was expected to exhibit low machining accuracy at the bottom surface.

From the results of the machinability and the machining accuracy tests, we confirmed that the difference in the elastic moduli of the polymer blanks based on the chemical structure (the RNC *vs.* PICN structures) and the difference in the inorganic filler content (the PMMA-based *vs.* hybrid composite resin groups) are expected to affect the machinability and the machining accuracy. However, a further investigation is required to explain the relationship of the merlon fracture test with various wall thicknesses and the mechanical properties of the blank.

In the visualization images of the deviation between CRD and CSD of the samples from each experimental group, a large portion of the merlon area and the bottom edge regions of the YHP, HPB, and VMT groups was yellow. In addition, we found the dark yellow region at the lower part of the merlon from the image of the VMT group. The PMMA CAM blocks used in this study either did not include inorganic fillers or contained a small amount of fillers. During the machining process in the CAD/CAM system, the block may have been deformed due to overheating caused by the high-speed rotation of the milling bur. As this overheating occurred intensively at the tip of the milling bur, the deviation at the bottom edge of the specimen was higher than that in other areas. Also, the thickness of the merlon wall (0.1–0.3 mm) is thinner than that of the bottom wall (2.0 mm). Thus, as the direction of the milling bur was parallel to the merlon wall, the merlon wall machined by the body of the bur appeared to have more machining errors than the bottom wall.

In addition, we observed a large portion of yellow color at the lower part of the merlon area and the bottom edge of the VEN group compared to the images of the VMD and SHC groups, similar to the results of the RMS values of the VEN group. The VEN hybrid block with a high-strength PICN structure has a high brittleness value. Therefore, the lower part of the merlon area and the bottom edge of the model are in vertical contact with the tip of the milling bur during the machining process, so the VEN group resulted in relatively low machinability compared to the VMD and SHC groups.

In terms of the limitation of this study, we evaluated the machinability and machining accuracy of polymer-

based CAD/CAM blocks by comparing designed STL and scanned STL files only. Therefore, the measurements of the actual wall thickness of the merlon model using a thickness gauge will be more helpful in confirming the results of the machinability and machining accuracy of polymer-based CAD/CAM blocks obtained from the current study.

CONCLUSION

We evaluated the machinability and machining accuracy of polymer-based CAM blocks using the merlon fracture test model specified in ISO 18675: 2022. In summary, there was a significant difference between the machinability and machining accuracy of different dental polymer-based CAD/CAM blocks according to different machining thicknesses and block types. Moreover, the amount and supporting structure of the inorganic filler included in the CAM blocks played an important role in the machinability and machining accuracy. Therefore, we conclude that the machining accuracy of CAM blocks should be determined *via* machinability and accuracy tests to produce accurate dental products. Additionally, we expect that the machinability and machining accuracy results of polymer-based CAM blocks can provide objective indicators for treatment plans in dental practice.

ACKNOWLEDGMENTS

This paper was supported by Wonkwang University in 2022.

REFERENCES

1) Coldea A, Swain MV, Thiel N. Mechanical properties of polymer-infiltrated-ceramic-network materials. Dent Mater 2013; 29: 419-426.
2) Ruse ND, Sadoun MJ. Resin-composite blocks for dental CAD/CAM applications. J Dent Res 2014; 93: 1232-1234.
3) Awada A, Nathanson D. Mechanical properties of resin-ceramic CAD/CAM restorative materials. J Prosthet Dent 2015; 114: 587-593.
4) Ling L, Ma Y, Malyala R. A novel CAD/CAM resin composite block with high mechanical properties. Dent Mater 2021; 37: 1150-1155.
5) Spitznagel FA, Horvath SD, Guess PC, Blatz MB. Resin bond to indirect composite and new ceramic/polymer materials: A review of the literature. J Esthet Restor Dent 2014; 26: 382-393.
6) Edelhoff D, Beuer F, Schweiger J, Brix O, Stimmelmayr M, Guth JF. CAD/CAM-generated high-density polymer restorations for the pretreatment of complex cases: A case report. Quintessence Int 2012; 43: 457-467.
7) Rayyan MM, Aboushelib M, Sayed NM, Ibrahim A, Jimbo R. Comparison of interim restorations fabricated by CAD/CAM with those fabricated manually. J Prosthet Dent 2015; 114: 414-419.
8) Perea-Lowery L, Minja IK, Lassila L, Ramakrishnaiah R, Vallittu PK. Assessment of CAD-CAM polymers for digitally fabricated complete dentures. J Prosthet Dent 2021; 125: 175-181.
9) Al-Dwairi ZN, Tahboub KY, Baba NZ, Goodacre CJ, Ozcan M. A comparison of the surface properties of CAD/CAM and conventional polymethylmethacrylate (PMMA). J Prosthodont 2019; 28: 452-457.
10) Soeda Y, Kanazawa M, Arakida T, Iwaki M, Minakuchi S. CAD-CAM milled complete dentures with custom disks and prefabricated artificial teeth: A dental technique. J Prosthet Dent 2022; 127: 55-58.
11) Takaichi A, Fueki K, Murakami N, Ueno T, Inamochi Y, Wada J, *et al*. A systematic review of digital removable partial dentures. Part II: CAD/CAM framework, artificial teeth, and denture base. J Prosthodont Res 2022; 66: 53-67.
12) Edelhoff D, Schweiger J, Prandtner O, Trimpl J, Stimmelmayr M, Guth JF. CAD/CAM splints for the functional and esthetic evaluation of newly defined occlusal dimensions. Quintessence Int 2017; 48: 181-191.
13) O'Brien WJ. Dental materials and their selection. 4th ed. Chicago: Quintessence Publishing; 2008.
14) Acar O, Yilmaz B, Altintas SH, Chandrasekaran I, Johnston WM. Color stainability of CAD/CAM and nanocomposite resin materials. J Prosthet Dent 2016; 115: 71-75.
15) Steier VF, Koplin C, Kailer A. Influence of pressure-assisted polymerization on the microstructure and strength of polymer-infiltrated ceramics. J Mater Sci 2013; 48: 3239-3247.
16) Arocha MA, Basilio J, Llopis J, Di Bella E, Roig M, Ardu S, *et al*. Colour stainability of indirect CAD-CAM processed composites vs. conventionally laboratory processed composites after immersion in staining solutions. J Dent 2014; 42: 831-838.
17) Lebon N, Tapie L, Vennat E, Mawussi B. Influence of CAD/CAM tool and material on tool wear and roughness of dental prostheses after milling. J Prosthet Dent 2015; 114: 236-247.
18) Miyazaki T, Hotta Y, Kunii J, Kuriyama S, Tamaki Y. A review of dental CAD/CAM: Current status and future perspectives from 20 years of experience. Dent Mater J 2009; 28: 44-56.
19) Rekow ED. High-technology innovations —and limitations— or restorative dentistry. Dent Clin North Am 1993; 37: 513-524.
20) Tuntiprawon M, Wilson PR. The effect of cement thickness on the fracture strength of all-ceramic crowns. Aust Dent J 1995; 40: 17-21.
21) Wataha JC. Alloys for prosthodontic restorations. J Prosthet Dent 2002; 87: 351-363.
22) Sorensen SE, Larsen IB, Jörgensen KD. Gingival and alveolar bone reaction to marginal fit of subgingival crown margins. Eur J Oral Sci 1986; 94: 109-114.
23) Nesse H, Ulstein DMÅ, Vaage MM, Øilo M. Internal and marginal fit of cobalt-chromium fixed dental prostheses fabricated with 3 different techniques. J Prosthet Dent 2015; 114: 686-692.
24) Yara A, Goto S, Ogura H. Correlation between accuracy of crowns fabricated using CAD/CAM and elastic deformation of CAD/CAM materials. Dent Mater J 2004; 23: 572-576.
25) Chavali R, Nejat AH, Lawson NC. Machinability of CAD-CAM materials. J Prosthet Dent 2017; 118: 194-199.
26) Zhang Y, Chai H, Lee JJ, Lawn BR. Chipping resistance of graded zirconia ceramics for dental crowns. J Dent Res 2012; 91: 311-315.
27) Quinn GD, Giuseppetti AA, Hoffman KH. Chipping fracture resistance of dental CAD/CAM restorative materials: Part I: procedures and results. Dent Mater 2014; 30: e99-e111.
28) Miyazaki T, Nakamura T, Matsumura H, Ban S, Kobayashi T. Current status of zirconia restoration. J Prosthodont Res 2013; 57: 236-261.
29) Peng CC, Chung KH, Yau HT, Ramos V Jr. Assessment of the internal fit and marginal integrity of interim crowns made by different manufacturing methods. J Prosthet Dent 2020; 123: 514-522.
30) Paul N, Raghavendra Swamy KN, Dhakshaini MR, Sowmya S, Ravi MB. Marginal and internal fit evaluation of conventional

metal-ceramic versus zirconia CAD/CAM crowns. J Clin Exp Dent 2020; 12: e31-e37.
31) Son K, Son YT, Lee JM, Lee KB. Marginal and internal fit and intaglio surface trueness of interim crowns fabricated from tooth preparation of four finish line locations. Sci Rep 2021; 11: 13947.
32) Goujat A, Abouelleil H, Colon P, Jeannin C, Pradelle N, Seux D, *et al*. Marginal and internal fit of CAD-CAM inlay/onlay restorations: A systematic review of in vitro studies. J Prosthet Dent 2019; 121: 590-597 e3.
33) ISO. ISO 18675 Dental-Machinable Ceramic Blank. Geneva: International Standard Organization; 2022.
34) ISO. ISO/DIS 5139 Dentistry-Polymer-based composite machinable blanks. Geneva: International Standard Organization; 2022.
35) Kohorst P, Junghanns J, Dittmer MP, Borchers L, Stiesch M. Different CAD/CAM-processing routes for zirconia restorations: influence on fitting accuracy. Clin Oral Investig 2011; 15: 527-536.
36) Song D-B, Han M-S, Kim S-C, Ahn J, Im Y-W, Lee H-H. Influence of sequential CAD/CAM milling on the fitting accuracy of titanium three-unit fixed dental prostheses. Materials 2021; 14: 1401.
37) Arezoobakhsh A, Shayegh SS, Ghomi AJ, Hakimaneh SMR. Comparison of marginal and internal fit of 3-unit zirconia frameworks fabricated with CAD-CAM technology using direct and indirect digital scans. J Prosthet Dent 2020; 123: 105-112.
38) Vélez J, Peláez J, López-Suárez C, Agustín-Panadero R, Tobar C, Suárez MJ. Influence of implant connection, abutment design and screw insertion torque on implant-abutment misfit. J Clin Med 2020; 9: 2365.
39) Tamam E, Güngör MB, Nemli SK, Bilecenoğlu B, Ocak M. Effect of different preparation finishing procedures on the marginal and internal fit of CAD-CAM-produced restorations: A microcomputed tomography evaluation. J Prosthet Dent 2021; doi: 10.1016/j.prosdent.2021.10.029.
40) Negm EE, Aboutaleb FA, Alam-Eldein AM. Virtual evaluation of the accuracy of fit and trueness in maxillary poly (etheretherketone) removable partial denture frameworks fabricated by direct and indirect CAD/CAM techniques. J Prosthodont 2019; 28: 804-810.
41) Helal MA, Abd Elrahim RA, El-latif Zeidan AA. Comparison of dimensional changes between CAD-CAM milled complete denture bases and 3D printed complete denture bases: An in vitro study. J Prosthodont 2022; doi: 10.1111/jopr.13538.
42) Soltanzadeh P, Suprono MS, Kattadiyil MT, Goodacre C, Gregorius W. An in vitro investigation of accuracy and fit of conventional and CAD/CAM removable partial denture frameworks. J Prosthodont 2019; 28: 547-555.
43) Haddad C, Azzi K. Influence of the type and thickness of cervical margins on the strength of posterior monolithic zirconia crowns: A review. Eur J Gen Dent 2022; 11: 73-80.
44) Omori S, Komada W, Yoshida K, Miura H. Effect of thickness of zirconia-ceramic crown frameworks on strength and fracture pattern. Dent Mater J 2013; 32: 189-194.
45) Choi BJ, Yoon S, Im YW, Lee JH, Jung HJ, Lee HH. Uniaxial/biaxial flexure strengths and elastic properties of resin-composite block materials for CAD/CAM. Dent Mater 2019; 35: 389-401.